International Journal of Offshore and Coastal Engineering
Vol.9 | No. 2 | pp. 33 – 43 | November 2025
e-ISSN: 2580-0914

Submitted: June 4, 2025 | Revised: July 30, 2025 | Accepted: September 10, 2025

Operability Analysis During Topside Platform Removal with Dynamic Method Due to Wave Load

Muhammad Zakaria Al Amin[a*], Murdjito[a], Eko Budi Djatmiko[a] and Fajar Rachmadiarto[b]

[a)] Department of Ocean Engineering, Institut Teknologi Sepuluh Nopember, Surabaya, Indonesia
[b)] Marine Engineer, PT ZEE Indonesia, Jakarta, Indonesia
*Corresponding author: m.zakariaalamin@gmail.com

ABSTRACT

Topside removal is one of the main activities in the offshore platform decommissioning process, with one of the methods in this process being reverse installation-single lift. Corrosion, one of the common problem factors in steel structures, is used as a parameter to reduce the strength of topside structures. In the structural strength analysis with a thickness reduction of 1.5mm, the maximum unity check values for members and joints are 0.854 and 0.602, respectively. Meanwhile, the dynamic analysis results show that the hoisting line and sling tension increase with increasing wave height and period. The response to increasing tension due to wave loads increases exponentially. The beam seas loading direction produces the highest tension response due to the roll motion response to the crane barge. The shortest hoisting line influences tension due to the higher stiffness value, which results in velocity and acceleration in the topside movement as a pendulum, thereby increasing the snap force. This pattern also applies to the dynamic amplification factor (DAF) and factor of safety (FOS) sling values. The distribution fitting results on the DAF value, 3-Parameter Lognormal, is the correct distribution model with a correlation value 0.999. So, the operational operability in the range of conditions for this research model is 89.4%.

Keywords: *Decommissioning, Topside Removal, Wave Load, Lifting, Dynamic Amplification Factor.*

1. INTRODUCTION

The offshore oil and gas industry has developed in Indonesia since the 1970s with CINTA platform which is in the SES block (Southeast Sumatera) as the first offshore platform built in Indonesia [1]. Based on SKK Migas data for 2024, Indonesia currently has 113 units platform is no longer operational as described in Table 1. Offshore platforms as one of the offshore oil and gas production facilities generally have an operational period of 15-20 years. So that is the process decommissioning need to be done. Decommissioning An oil and gas platform is the process of removal and restoring all oil and gas production facilities, including wells, equipment, installations, and other supporting facilities after the cooperation contract ends [2]. This is part of efforts to maintain environmental sustainability and is included in the Indonesia Oil & Gas (IOG) 4.0 strategic plan. One of the main pillars is National Decommissioning Strategy, which includes designing and implementing management plans decommissioning effective and timely. To achieve these goals, technology and methods are developed decommissioning that is effective and efficient is very necessary. Process decommissioning, such as demolition (removal), generally carried out offshore. On fixed platform, equipment at topside transferred to a barge before deck removal takes place, which may impact center of gravity (COG) [3]. The commonly used method is heavy lifting by using Heavy Lift Vessel (HLV) both single lift or partial removal with crane barge. However, surgery lifting requires relatively calm environmental conditions to be carried out, with certain restrictions to reduce the risks that occur due to the movement of the ship and the surrounding environment.

Table 1. inactive offshore oil and gas platforms based on age and platform type in Indonesia [4]

Platform Type	Structure Age (years)						*Total*
	<15	15-20	20-30	30-40	>40	-	
Braced Monopod	1	1	6	1	1	3	***13***
1 leg Caisson	0	0	1	4	12	0	***17***
Jacket 3 legs	0	1	5	21	33	0	***60***
Jacket 4 legs	0	0	1	7	8	0	***16***
Jacket 6 legs	0	0	0	1	0	0	***1***
Jacket template	0	0	0	1	2	0	***3***
Caisson-Pile (4legs)	0	0	0	0	1	0	***1***
Unknown	0	1	0	0	1	0	***2***
Total	***1***	***3***	***13***	***35***	***58***	***3***	***113***

The strength of aged offshore structures must consider corrosion factors, fatigue cracking, local dents, and other damage conditions[5].Corrosion is important when considering structural design analysis because corrosion

significantly influences material degradation [6]. In offshore structures, the level of corrosion increases linearly in steel structural parts in the atmospheric and submerged zones as the structure ages [7]. Reducing the thickness of the structure results in reduced integrity. Reduction in thickness due to corrosion results in an increase in von mises stress on the web plate girder [8]. The reduction in thickness due to corrosion of the steel material has a linear effect on the strength of the structure as the age of the platform increases[9]. Although the influence of corrosion in the atmospheric zone on the global strength of the structure is not significant, in removal operations, it is important to still evaluate the strength of the structure at the lifting point (lift point) to be able to evaluate failure scenarios that occur [10].

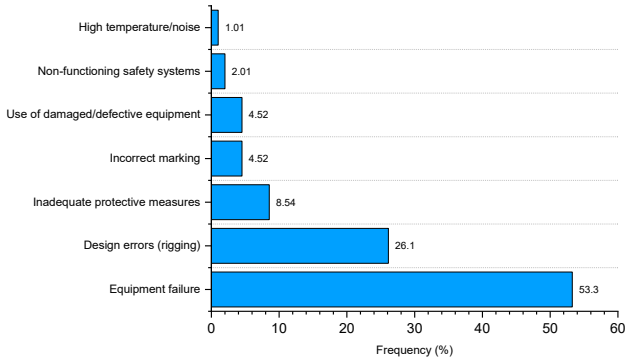

Figure 1. Causes of accidents in offshore lifting operations - Technical Operability [11]

The vessel movement affects the dynamic load on offshore lifting operations. According to [12], the operating performance of a floating crane vessel is influenced by the vessel's dynamic forces on the environment and loads from the module that was appointed. So, a large dynamic load that works during the lifting process may increase due to the response factors it receives. The integrity of the lifted structure will suffer von Mises stress differently in the direction of environmental loading towards the crane barge [13].

Lifting operation is also affected by environmental loads and vessel movements that increase tension on the sling connected to the pendulum[13]. Motion response crane barge is influenced by the module lifted during operation and resonance in movement surge and yaw [14]. The heavier weight of the pendulum (the object being lifted) causes the pendulum to move, and the crane tip motion is so that the ship's motion responds to movement heave and roll increase [15].The tension in the lines during operation lifting experienced a linear increase in response to increasing wave height loads [12].

On vessel movements heave, the value of DAF tends to increase in stepped lifting [16]. Meanwhile in research [12], movement roll on a floating crane during operation has almost twice as much influence on the system in the module at 6 degrees of freedom (6DOF) movement than 3 degrees of freedom (3DOF). Wave height and wave period in research [17], significantly influence the structural response, linear with the RAO of the motion response floating structure. The largest DAF on operations lifting well in condition lift off, in air, through the splash-zone, and close to seabed influenced by movement roll in the direction of the environmental load beam seas [18].

This research analyzes critical aspects of operations, including topside removal on an offshore platform. This research will evaluate the structural strength integrity topside during lifting. In addition, this research will examine the tension response on sling and hoisting lines, which is influenced by variations in wave conditions. These variations in wave conditions can impose significant loads and affect the tension of the lifting equipment. Finally, this research will examine the value of Dynamic Amplification Factor (DAF) and operational operability, which are also affected by changes in wave load.

2. THEORY

2.1 Hoisting System

The crane's hoisting system allows it to lift objects weighing more than the capacity of one line. This system usually uses multiple lines, so the connection from the crane tip to the block generally has more than one line. According to [18], the following equation (1) can be used to calculate the stiffness of the hoisting system.

$$\frac{1}{K} = \frac{1}{k_{rigging}} + \frac{1}{k_{line}} + \frac{1}{k_{soft}} + \frac{1}{k_{block}} + \frac{1}{k_{boom}} + \frac{1}{k_{other}} \quad (1)$$

Meanwhile, the stiffness of the line is calculated using equations (2) and (3) below.

$$k_{line} = \frac{EA}{L}[N/m] \quad (2)$$

$$A_{line} = \frac{\pi \cdot D^2}{4} \cdot c_f \quad (3)$$

By substituting equations (2) and (3), the stiffness value of the parallel hoisting line can be calculated using the equation (4) below.

$$k_{total} = \frac{E \cdot \pi \cdot D^2 \cdot c_f}{4 \cdot L} \cdot n \quad (4)$$

2.2 Dynamic Amplification Factor

The dynamic amplification factor (DAF) accounts for global dynamic effects resulting from vessel motions, boom, wire, and rigging stiffness, boom tip location and motions, crane movements, and wind loading [20]. Conventionally, DAF can be calculated using equation (5), the ratio of the largest total force on the system with the object mass in the air multiplied by the acceleration due to gravity.

$$DAF_{conv} = \frac{F_{total}}{Mg} \quad (5)$$

2.3 Corrosion

Corrosion is a material degradation process, especially in metals, that occurs due to direct contact with the

environment (water and air) or other chemical processes. As a simplification in analysis, the strength of members is assumed to have uniform thickness reduction throughout the member [21]. The corrosion rate in steel structures, according to [7], can be seen in Table 2.

Table 2. Typical corrosion rates in offshore structures [7]

Environmental Condition	Corrosion Rate (mm/year)
Submerged steel specimens, in seawater conditions	0.05-0.20
Pile	0.08
Tidal zone	0.10-0.25
Atmospheric zone	0.05-0.10
Ship deck without protective coating	0.10-0.50

2.4 Hydrodynamic of Rectangular Box

In the rectangular box geometry, [22] uses C_d for the force in the flow, so $C_d = C_x$. Meanwhile, for the drag properties in rotational movements, there is no standard data source, so in the computational process [23], assumes that the contribution of the drag force df to the element area dA uses equation (6) where the value of C_d is assumed to be the same for all points on the surface.

$$df = \frac{1}{2}\rho|v|^2 C_d \, dA \tag{6}$$

$$df = \frac{1}{2}\rho\omega z|\omega z| C_d \, x \, dz \tag{7}$$

$$dm = \frac{1}{2}\rho\omega z|\omega z| C_d \, x \, dz \, z \tag{8}$$

$$dm = \frac{1}{2}\rho\omega|\omega| C_d \, x \, z^3 \, dz \tag{9}$$

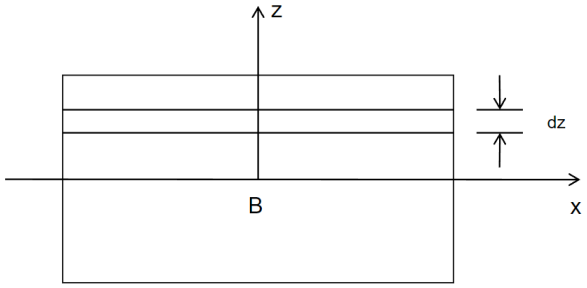

Figure 2. Integration for drag and rotation properties [23]

2.5 Time Domain Analysis

Lifting operations can be analyzed through time-domain simulations based on the wave excitation force transfer function, which depends on the pre-generated frequency, added mass, and wave damping for the crane vessel, transport barge, and lifted object [19] Using numerical integration, time-domain analysis can be utilized to solve the floater response in the time domain.

$$\sum_{j=1}^{6}\{(M_{ij} + a_{ij}).\ddot{x} + \dot{b}.x + c.x\} = F_i \text{ for } i = 1\sim6 \tag{10}$$

$$F = F_m + F_w + F_l \tag{11}$$

The static weight of the topside and rigging is estimated to be 696.31 MT. According to [19] this weight is categorized as a light lift because the weight of the lifted object is less than 2% of the vessel's displacement (2% of the crane barge displacement is 1010 MT). In light lift scenarios, the motion characteristics of the vessel at the crane tip are not influenced by the lifted object[19]. Therefore, in light lift modeling terminology for OrcaFlex analysis, the vessel's motion is modeled using displacement RAO [24]. The simulation is conducted for 30 minutes based on a sensitivity study[19]. The analysis results are then used to obtain extreme value statistics with a Rayleigh distribution to determine the maximum possible value during a 3-hour analysis [19].

3. METHODOLOGY

The research flowchart process is described in Figure 3. The data in this research used topside with a wellhead platform type as described in Table 3. The decommissioning process chosen was a single lift with the reverse installation method. The operating vessel used is a crane barge with specifications in Table 4 with the crane capacity presented in Figure 4. The hoisting system on the crane is parallel lines with a total number of lines of 52. Detailed specifications of the hoisting line can be seen in Table 5. Dynamic simulations are carried out using variation of colinear loading direction with the wind spectrum recommended by [25] is NPD spectrum. Time-domain analysis was carried out on fully licensed OrcaFlex Version 11 software owned by PT. ZEE Indonesia with details of the variations in this study are illustrated in Figure 5 and Table 6.

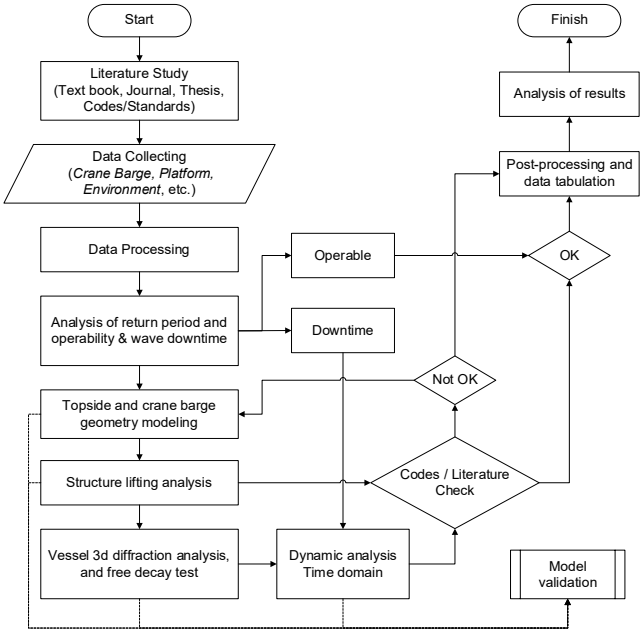

Figure 3. Flowchart of methodology

Table 3. Topside general data

Parameter	Description
Name	XYZ platform
Type	Wellhead platform
Weight	688.64 MT

Parameter	Description
Design life	15 years

Table 4. Crane barge general specification

Parameter	Value	Unit
Length overall	169	m
Breadth overall	46	m
Depth	13.5	m
Volume displacement	58857.5	m^3
Displacement	60498.9	MT
Draft	8.528	m
Trim, AP	-2.496 (1.69)	m (deg)
Heel, PS (+)	0	deg

Table 5. Hoisting line specification

Parameter	Value	Unit
Diameter	60	mm
Total Length	2900 x 2	m
Reeving part	2 x 26	-
Structure	6xK3WS - IWRC	-
Grade	1960	N/mm^2
Breaking Load	301	MT
Young's Modulus	$85x10^9$	N/m^2
Main Hook Weight	42.5	MT

Table 6. Load case and load variation

Parameter	Value	Unit
Significant wave height, Hs	1.0-3.5(1)	m
Wave period, Tz	7 dan 8	s
Wave spectrum	ISSC	-
Wind speed, U_{10}	17.9	m/s
Wind spectrum	NPD	-
Environment load heading	0-180(2)	deg
Hoisting line length	20-40(3)	m

(1) the increment of Hs variation is 0.5m
(2) the increment of environment heading is 45deg
(3) hoisting line length increment is 5m

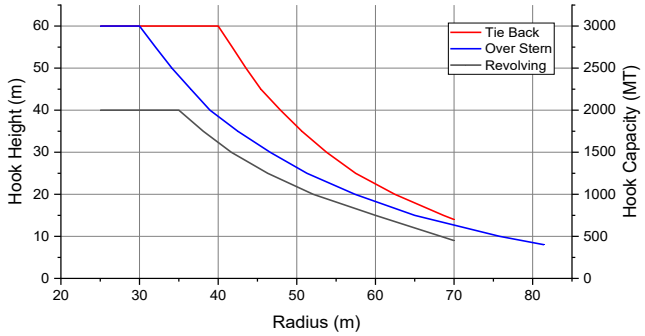

Figure 4. Crane capacity

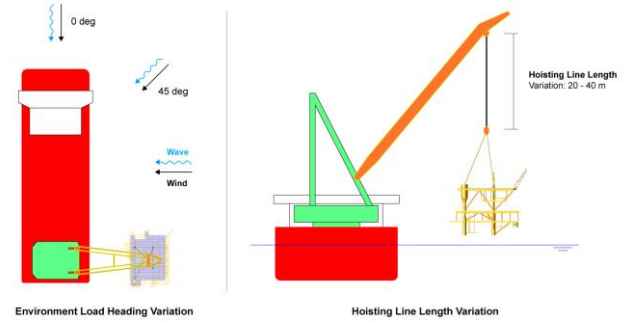

Figure 5. Illustration of load variation

4. RESULTS

4.1 Study Case Location

The case study location for this research was the Natuna Sea, approximately 234km WNW (west-northwest) from the Riau Islands. This location is at latitude 4.32° and longitude 106.08°. It has a depth of 79 meters in the open sea directly adjacent to the Gulf of Thailand and the South China Sea. With these geographical conditions, based on the rule of thumb explained by [26] the wave spectrum characteristics in these waters are Pierson-Moskowitz or ISSC.

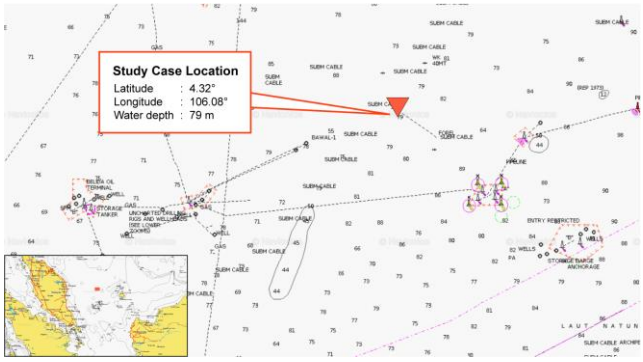

Figure 6. Study Case Location, modifed form [27]

4.2 Rigging Design

The topside is modelled to be corroded by 1.5 mm according to the corrosion rate in Table 2 for 15 years according to the design life of the platform. So, the weight of the structure has been reduced to 613.55 MT. Rigging calculations are based on calculations and factors according to [20]. The design DAF value on the topside is 1.20 based on [20]. A summary of the rigging design can be seen in Table 7. The sling size was 260mm with FOS 5,554, and the total static weight of the topside, including rigging, was 696.31 MT.

Table 7. Rigging design summary

Parameter	Value	Unit
Structure Weight	613.66	MT
DAF	1.20	-
WCF	1.10	-
Number of Slings	4	ea
Sling Diameter	260	mm
MBL Sling	2785	MT
Sling Type	Cable Laid	-
Sling Weight	0.237	MT/m
Number of Shackle	4	ea
Shackle Type	P-6036	-
Shackle Weight (per 1 shackle)	1.28	MT
Static Weight (include rigging)	696.31	MT
Nominal FOS	5.554	-

4.3 Structural Integrity

Strength analysis of the topside justification structure is based on [28] and [29] with the equation of unity check on members as follows.

$$UC = \frac{\sigma_{act}}{\sigma_{perm}} \quad (12)$$

Due to the inaccuracy of the COG point, this lifting analysis is modelled using COG shift by applying a force to the lift point due to the shift of the hook point on the COG envelope.

Table 8. Force at Lift Point due to COG Shifting

COG Envelope Position	Force at joint due to COG Shift (kN)			
	P001	P002	P003	P004
CoG Shift #1 (+X+Y)	31.72	-423.39	-31.72	423.39
CoG Shift #2 (-X+Y)	-423.39	31.72	423.39	-31.72
CoG Shift #3 (-X-Y)	-31.72	423.39	31.72	-423.39
CoG Shift #4 (+X-Y)	423.39	-31.72	-423.39	31.72

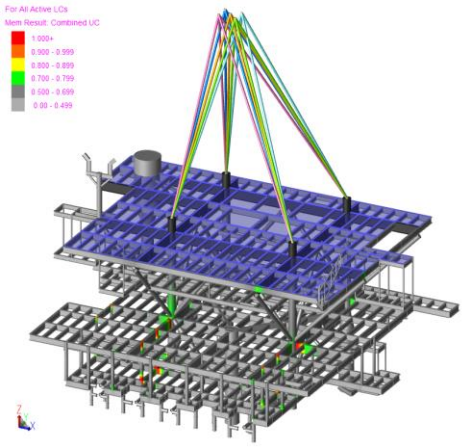

Figure 7. Unity Check Plot at Member

Table 9. Maximum Unity Check Summary

Parameter	UC
Member connected to lift point	0.854
Member unconnected to lift point	0.830
Joint	0.601

4.4 Decay Test

Decay tests are carried out to obtain the natural period of motion of the floating structure in free-floating conditions. Decay tests are carried out on primary floating structure motion, namely roll, pitch and heave. The results of the decay test are graphically shown in Figure 8. The natural period is processed using the maxima-minima method, namely, getting the maximum and minimum peaks of the decay response. The distance between 1 amplitude is then processed to obtain the natural period of motion. In the heave motion, the natural period is found at 8.78 seconds. Meanwhile, in the roll motion, the natural period is 10.29 seconds. In the pitch motion, the natural period is 8.63 seconds.

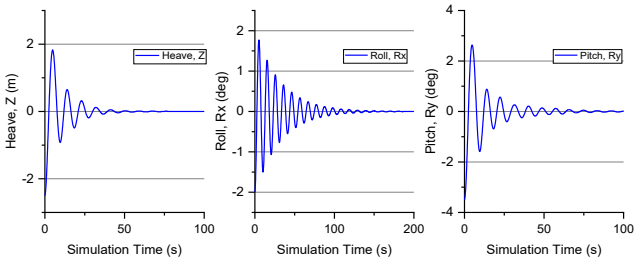

Figure 8. Free Decay Test

4.5 Hoisting Line Stiffness

The stiffness of the hoisting line is calculated based on equation (4). From this equation, the stiffness value of the hoisting line is obtained in Figure 9. The stiffness graph depicts the relationship between stiffness (in units of kN/m) and the length of the hoisting line in the distance between the crane tip and the crane block. The stiffness value increases exponentially with the shortening of the length of the hoisting line. This phenomenon may be caused by the load distribution and mechanical properties of the hoisting line, where the hoisting line is stiffer at short distances due to minimal bending or strain effects, while at longer distances, the hoisting line experiences more strain and deformation.

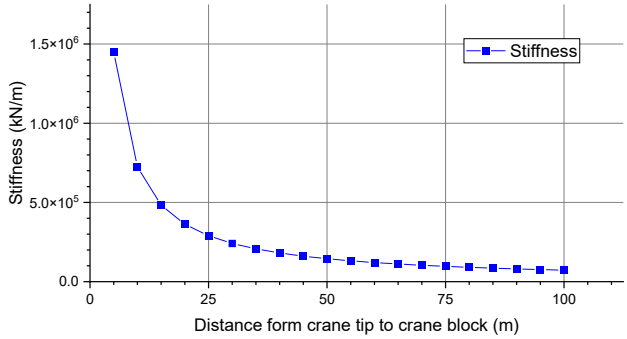

Figure 9. Hoisting Line Stiffness.

4.6 Hydrodynamic of Topside

The topside model is simplified by representing the model as a solid prism with a Lumped 6D Buoy on the OrcaFlex. Equipment, pipes, or asymmetrical topside geometric shapes are not modelled in detail and then transformed into simple prisms as a geometric interpretation of the topside structure in the OrcaFlex model, as illustrated in Figure 10. The topside model in OrcaFlex is modelled numerically with dynamic loading simultaneously acting inertia and drag on the topside.

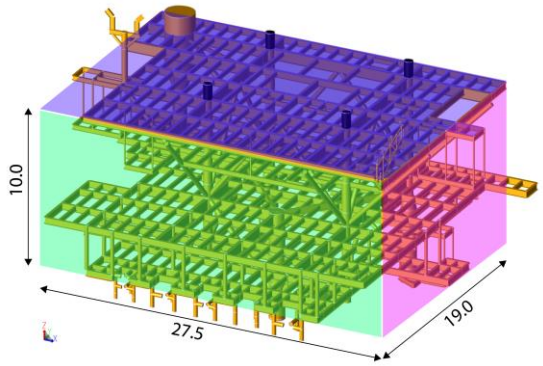

Figure 10. Illustration of Simplified Topside Model to Prism Geometry.

The property of the simplified topside is that it is a roughly rectangular prism, so according to [30], the value of C_D = 2.05. A summary of the properties of the topside as input to OrcaFlex is described in Table 10 below.

Table 10. Topside Hydrodynamic Properties

Parameter	Value	Unit
Length, l_x	27.5	m
Width, l_y	19.0	m
Height, l_z	10.0	m
COG, x, y, z	-1.27, -2.28, 9.33	m
Mass (WCF)	675.026	MT
Drag Area X, A_x	270.0	m^2
Drag Area Y, A_y	190.0	m^2
Drag Area Z, A_z	522.5	m^2
Mass moment inertia X, I_x	25932.24	$MT.m^2$
Mass moment inertia Y, I_y	48165.91	$MT.m^2$
Mass moment inertia Z, I_z	62847.73	$MT.m^2$
Rotational Drag X, R_{dx}	242711.48	m^4
Rotational Drag Y, R_{dy}	659035.22	m^4
Rotational Drag Z, R_{dz}	423941.28	m^4
Volume	5225.0	m^3
Drag Coefficient, C_D	2.05	-

4.7 Tension on Hoisting Line and Sling

The results of the dynamic analysis simulation showed that the maximum tension occurred in the hoisting line and sling with dynamic analysis for 30 minutes. These results were carried out using extreme value statistics with the Rayleigh distribution to obtain the most significant possible maximum tension value during the 3-hour simulation. In Figure 11, the tension on the sling is linear against the pattern of increasing tension on the hoisting line. In this case, the greater the angle at the lift point or the longer the sling, the greater the tension.

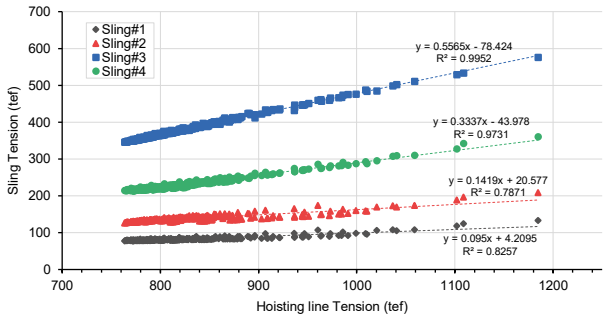

Figure 11. Correlation of tension value between hoisting line and slings.

The tension on the hoisting line and sling increases steadily, and the response pattern is similar in wave heights of 1.0 m to 3.5 m. In the wave period, the tension response also increases as the wave period increases from Tz = 8 seconds to Tz = 9 seconds. The highest tension in varying loading directions occurs in the beam seas or 90-degree direction.

If seen from the PSD results in Figure 13 and Figure 14, the crane barge movement's response directly influences the environmental load applied. In the head and following sea directions, the tension is influenced by the crane barge's surge, heave and pitch movements. Meanwhile, the tension is influenced by heave, roll and pitch motion in the quartering seas and beam seas directions. The beam seas loading direction has the most significant influence on increasing the tension on the hoisting line. Roll motion has the most significant energy in PSD from the results of spectrum analysis using the FFT method obtained so that the most significant influence of increasing tension on the hoisting line and sling on the motion response of the crane barge is roll, followed by heave and pitch which also have a contribution, but the energy provided is not the size of a roll.

Another influence on the tension in the hoisting line and sling is the velocity and acceleration of movement from the topside. In PSD, these parameters contribute to both the first and second peaks. This velocity and acceleration causes a snap force in the lines, significantly increasing the tension, as explained in [19]. In the snap force, the shorter the hoisting line, the greater the stiffness value, and it is directly proportional to the increase in velocity response and movement acceleration from the topside movement. Thus, the snap force that occurs becomes greater.

4.8 Dynamic Amplification Factor

The DAF value is calculated using equation (5) by dividing the maximum tension on the hoisting line by the static weight of the lifting system. The OrcaFlex model's static weight model includes the topside, crane block, and rigging, with a total weight of 752.86 MT. In Figure 12, the DAF value increases with shorter hoisting line lengths (20m), followed by increasing wave height and period. With variations in the direction of environmental loading, the

DAF value increases in the direction of environmental loading at 90 degrees (beam seas). It decreases in head-following seas, followed by an increase in wave height and period. The DAF value = 1.20 is used as a limit in Figure 14. Considering variations in hoisting line length and loading direction, the maximum limit of significant wave height permitted at Tz = 8s is 1.87m, while at Tz = 9s is 1.66m.

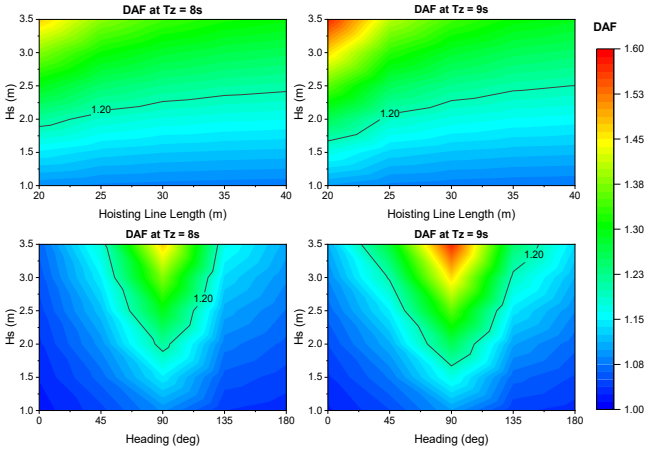

Figure 12. Dynamic Amplification Factor

In Figure 15, the value of the factor of safety (FOS) on the vulnerable sling decreases as the length of the hoisting line becomes shorter, followed by an increase in wave height and period. With variations in environmental loading, the FOS value decreases in the direction of environmental loading of 90 degrees (beam seas). It increases in head-following seas, followed by an increase in wave height and period. The minimum FOS sling value from the rigging design results is 5.55. The contour plot shows that with the design FOS limits if considering variations in hoisting line length and environmental load direction, the maximum significant wave height limit at Tz = 8s is 3.04m, while at Tz = 9s is 2.68m.

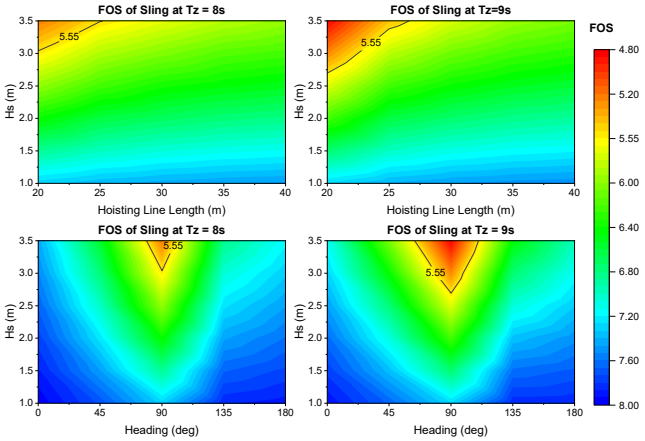

Figure 15. Sling Safety Factor

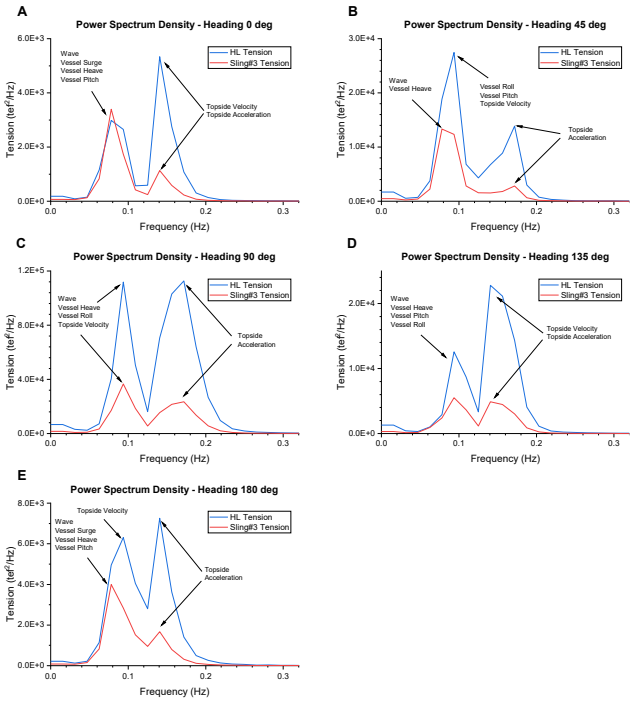

Figure 13. PSD of heading variation

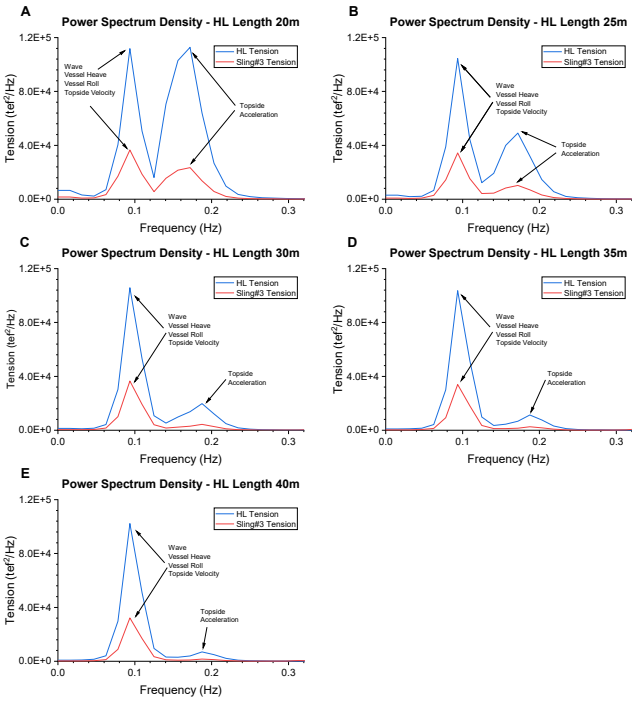

Figure 14. PSD of hoisting line length variations

4.9 Sling Safety Factor

4.10 Crane Capacity Safety Factor

The crane capacity can be seen in Figure 4. The crane capacity is in a revolving condition because the object's position is on the starboard side in the simulation model. In Figure 16, the crane capacity factor of safety (FOS) decreases at the most extended hoisting line length (40 meters), followed by an increase in wave height and period. When varying the direction of environmental loading, the FOS value of the crane decreases in the direction of environmental loading of 90 degrees (beam seas). It increases in head-following seas, followed by an increase in wave height and period. The minimum FOS at crane capacity is 1.02. With a capacity limit of 1.0, the crane is considered safe even if the hoisting line length variation is 40 meters and the FOS has a critical area (red).

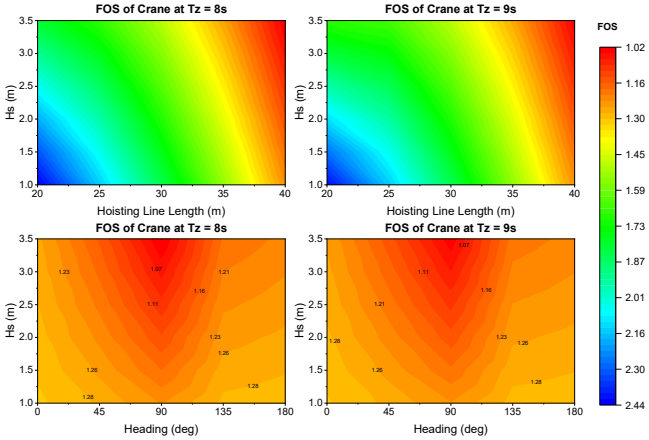

Figure 16. Crane Capacity Safety Factor

4.11 Wave Load Response

In no-load environmental conditions, the maximum tension occurs at the crane tip on the hoisting line. The tension in the hoisting line is equal to the static weight of the model. That is because the topside is in the air, so there is no buoyancy force on the topside. Equation (5) is used to find the DAF value, which is a comparison between the maximum tension that occurs divided by the static weight of the model. The significance of the influence of wave loads or the environment is linear on the DAF value.

The graph in Figure 17 shows that the maximum tension response due to wave loads increases with increasing wave height. The response caused by the wave load increases linearly with a significant increase in wave height with power regression. The power regression curve in this graph shows the relationship between wave height and maximum tension response at HL. The power regression curve for Tz = 8s and Tz = 9s shows the exponential relationship between wave height and maximum tension response.

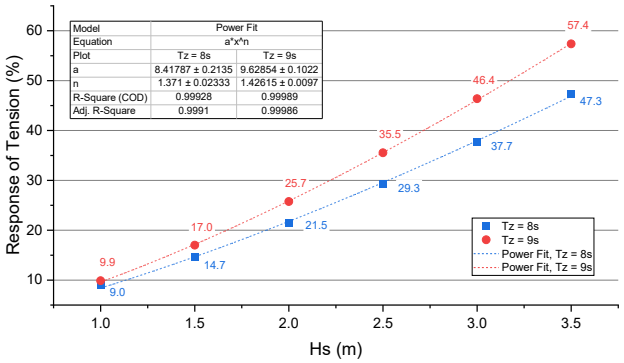

Figure 17. Maximum response of tension due to wave load

The regression parameters shown in this graph provide information about the relationship between wave height and the maximum response of the structure. The regression coefficient (a) shows the magnitude of wave height's influence on the structure's maximum response. The regression exponent (n) shows how the influence of wave height on the maximum response of the structure changes with changes in wave height. The coefficient of determination (R-Square and Adj. R-Square) shows how well the power regression curve can explain the relationship between wave height and maximum response of the structure with values for both 0.999. At Tz = 8s, the tension response increases by 9.0% at Hs = 1.0m and 47.3% at Hs = 3.5m. At Tz = 9s, the tension response increases by 9.9% at Hs = 1.0m and 57.4% at Hs = 3.5m.

4.12 Probability Distribution Model

Distribution fit is carried out on the results of the DAF values to obtain a distribution model of the sample results of the DAF values against a particular distribution. At this stage, probability fitting is achieved by obtaining goodness of fit and index of fit values using the least squares method. The results of the distribution suitability test on the DAF value results show that the correct distribution is the 3-parameter Lognormal distribution illustrated in Figure 18 with an Anderson Darling (adj) value of 0.190 and a correlation coefficient value of 0.999.

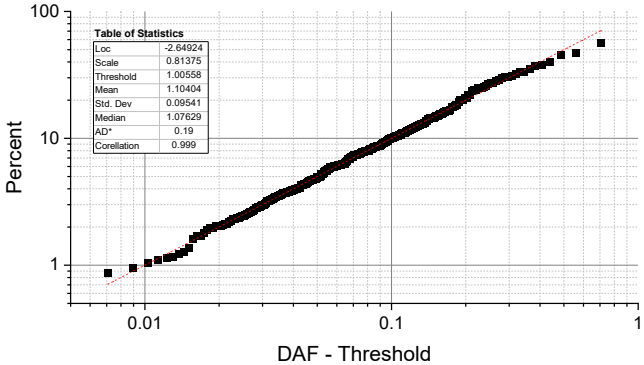

Figure 18. DAF value with 3-Parameter Lognormal with distribution fit

The study results are compared to those of previous research to validate the distribution model. Similar research was taken from [18], [31], and [32] with DAF results on conditions of objects in the air. The wave parameters, ship type, ship ratio, and weight and geometry of the objects from this comparison have nothing in common.

From Table 11, it can be concluded that of the 6 data tested, 5 of these data gave 3-Parameter Lognormal distribution results, which is the most suitable distribution model to be used as a DAF value distribution model even though the variables and data studied have many differences. In research [18], the most appropriate distribution model was a 3-parameter logistic with a goodness of fit value of 1.488. However, the goodness of fit value of research [18] on 3-Parameter Lognormal is 1.722. The difference in the goodness of fit value of the two distributions is 0.234. So, the 3-parameter Lognormal distribution model as a DAF distribution model can be considered acceptable considering the authors and other research results.

Table 11. Goodness of fit distribution results

Distribution	Result	Madland	Viki	Eri Sandra		
				289MT	400MT	600MT
3-P Weibull	1.834	6.306	9.283	0.811	0.537	0.568
3-P Lognormal	**0.190**	1.722	**2.785**	**0.273**	**0.376**	**0.467**
3-P Loglogistic	0.517	**1.488**	3.479	0.664	0.943	1.055
2-P Exponential	3.060	19.065	13.861	1.467	2.361	5.685

4.13 Operability

Table 12 summarizes the results of the criteria analysis. From the structural strength analysis results, the UC value meets the criteria with a design DAF = 1.20 in accordance with [20]. However, in the dynamic analysis results, the DAF value shows that 34 out of 300 simulations do not meet the criteria with a DAF value of more than 1.20 compared to other variables against the criteria. Therefore, DAF is the main factor in determining the operability criteria for this operating system.

Table 12. Summary of analysis results on operability criteria.

Parameter	Criteria		OK	NOT OK
Structure Strength	UC	<1.00	OK	-
DAF	Nilai	<1.20	266	34
Sling	FOS	>5.55	295	5
Crane Capacity	FOS	>1.00	300	0

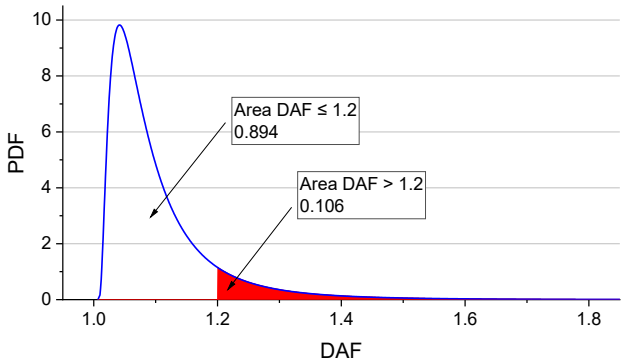

Figure 19. Probability density function of DAF

The statistical value of the 3-parameter Lognormal distribution from the fitting results is shown in Figure 18. The data is processed to obtain a probability density function or PDF. Figure 19 shows that with the design DAF value = 1.20 as the operability limit parameter, the PDF area with DAF > 1.20 is 0.106. Meanwhile, the PDF area with DAF ≤ 1.20 is 0.894. So, the operability of the operating system in this study was 89.4%, and downtime was 10.6% at significant waves of 1.0-3.5 m and a zero up-crossing (Tz) period of 8-9 seconds. The operating limit with the operational sequence model, as in this study, is that the significant wave height at Tz = 8s is 1.87m, while at Tz = 9s, it is 1.66m.

5. CONCLUSION

The topside structure has sufficient strength and integrity to remove if corroded by 1.5mm (15 years of design). The maximum UC value is 0.854 for members connected to the lift point and 0.830 for members not connected to the lift point, while the maximum joint UC is 0.60. Thus, the structural integrity still has strength within safe limits for removal (lifting) operations.

The tension on the hoisting line and sling increases exponentially with significant increases in wave height and wave period. The response to increasing tension due to wave loads increases exponentially. The maximum tension on the hoisting line is 1184.8 tef, while on the sling, it is 576.5 tef. The sling's most significant tension occurs on sling #3, namely on the sling with the most significant angle to the center of the hook point. When varying the direction of loading, the highest tension occurs at a heading of 90 degrees (beam seas). Meanwhile, with variations in hoisting line length, the tension increases with the shortness of the hoisting line, with critical tension occurring at 20 meters. The tension on the hoisting line and slings is influenced by the response of the ship's motion, with roll motion contributing to the most significant increase in tension, as well as the velocity and acceleration of topside motion, which results in snap forces on the hoisting line and slings. The lowest FOS at crane capacity is 1.02, which occurs on a 40m hoisting line.

The DAF value increases significantly with increases in wave height and wave period. The most extensive DAF value result is 1.57. The pattern of increasing DAF is also caused by the short hoisting line and the environmental loading direction of 90 degrees. The distribution fitting results from the DAF values show that the 3-parameter Lognormal distribution is a suitable distribution model with a correlation value 0.999. With this distribution, the resulting probability density function for the operability of a DAF value of less than 1.20 is 89.4%. The significant wave height limit at Tz = 8s is 1.87m, while at Tz = 9s, it is 1.66m.

REFERENCES

[1] E. Arianti and A. Ghofur, "Teknologi Decommissioning Anjungan Lepas Pantai Terpancang Pasca-Operasi," *JURNAL INOVTEK POLBENG*, vol. 9, no. 2, 2019.

[2] KESDM, *PERMEN ESDM Nomor 15 Tahun 2018 Tentang Kegiatan Pasca Operasi pada Kegiatan Usaha Hulu Minyak dan Gas Bumi*. 2018.

[3] ICF International, "Decommissioning Methodology and Cost Evaluation," 2016.

[4] SKK Migas, "Data Inactive Offshore Platform di Indonesia," *Unpublished*. SKK Migas, Jakarta, 2024.

[5] D. K. Kim, M. A. Zalaya, M. H. Mohd, H. S. Choi, and K. S. Park, "Safety assessment of corroded jacket platform considering decommissioning event," *INTERNATIONAL JOURNAL OF AUTOMOTIVE AND MECHANICAL ENGINEERING*, vol. 14, no. 3, pp. 4462–4485, Sep. 2017, doi: 10.15282/ijame.14.3.2017.6.0353.

[6] M. M. A. Wahab, V. J. Kurian, M. S. Liew, and D. K. Kim, "Condition Assessment Techniques for Aged Fixed-Type Offshore Platforms Considering Decommissioning: a Historical Review," *Journal of Marine Science and Application*, vol. 19, no. 4, pp. 584–614, Dec. 2020, doi: 10.1007/s11804-020-00181-z.

[7] R. E. Melchers, "Corrosion uncertainty modelling for steel structures," *J Constr Steel Res*, vol. 52, no. 1, pp. 3–19, Oct. 1999, doi: 10.1016/S0143-974X(99)00010-3.

[8] Y. Sharifi, S. Tohidi, and J. K. Paik, "Ultimate compressive strength of deteriorated steel web plate with pitting and uniform corrosion wastage," *Scientia Iranica*, vol. 23, no. 2, pp. 486–499, Apr. 2016, doi: 10.24200/sci.2016.2133.

[9] N. A. Othman, M. H. Mohd, M. A. A Rahman, M. A. Musa, and A. Fitriadhy, "Investigation of the corrosion factor to the global strength of aging offshore jacket platforms under different marine zones," *International Journal of Naval Architecture and Ocean Engineering*, vol. 15, p. 100496, 2023, doi: 10.1016/j.ijnaoe.2022.100496.

[10] A. M. A. Abdelaah, S. M. Cresswell, G. M. E. Manzocchi, and C. Thistlethwaite, "Practical Applications of Structural Analysis Support to Decommissioning," in *Day 1 Mon, May 02, 2016*, OTC, May 2016. doi: 10.4043/27128-MS.

[11] K. Prøsch, "Risk in crane and lifting operations related to the logistic interaction process for well and drilling.," Master Thesis, Norwegian University of Science and Technology, Torgarden, 2011.

[12] J.-H. Cha, M.-I. Roh, and K.-Y. Lee, "Dynamic response simulation of a heavy cargo suspended by a floating crane based on multibody system dynamics," *Ocean Engineering*, vol. 37, no. 14–15, pp. 1273–1291, Oct. 2010, doi: 10.1016/j.oceaneng.2010.06.008.

[13] S.-H. Ham and M.-I. Roh, "Time-domain structural analysis during block turnover and lifting using 2D flexible multibody dynamics," *Marine Structures*, vol. 75, p. 102841, Jan. 2021, doi: 10.1016/j.marstruc.2020.102841.

[14] N. Firdaus, E. B. Djatmiko, R. W. Prastianto, and Muryadin, "Experimental Study on Coupled Motion of Floating Crane Barge and Lifted Module in Irregular Waves," *IOP Conf Ser Earth Environ Sci*, vol. 972, no. 1, p. 012070, Jan. 2022, doi: 10.1088/1755-1315/972/1/012070.

[15] G. O. Tysse and O. Egeland, "Dynamic Interaction of a Heavy Crane and a Ship in Wave Motion," *Modeling, Identification and Control: A Norwegian Research Bulletin*, vol. 39, no. 2, pp. 45–60, 2018, doi: 10.4173/mic.2018.2.1.

[16] H. Cao, X. Yan, J. Xia, and D. Wei, "Effect of fluid-structural interaction on the dynamic response of stepped lifting system subjected to heave motion," *Ocean Engineering*, vol. 279, p. 113943, Jul. 2023, doi: 10.1016/j.oceaneng.2023.113943.

[17] L. Li, Z. Gao, T. Moan, and H. Ormberg, "Analysis of lifting operation of a monopile for an offshore wind turbine considering vessel shielding effects," *Marine Structures*, vol. 39, pp. 287–314, Dec. 2014, doi: 10.1016/j.marstruc.2014.07.009.

[18] S. Madland, "Dynamic Analysis for the Installation of Offshore Wind Turbine Foundations," University of Stavanger, Stavanger, 2012.

[19] DNV, "DNVGL-RP-N103 Modelling and analysis of marine operations." Det Norske Veritas, Bærum, 2017.

[20] DNV, "DNV-ST-N001: Marine Operations and Marine Warranty." Det Norske Veritas, Bærum, 2023.

[21] NORSOK, "NOSROK N-004 Design of Steel Structure." Norwegian Technology Standards Institution, Oslo, 1998.

[22] ESDU, "ESDU 71016: Fluid forces, pressures and moments on rectangular blocks.," *ESDU International*, 1978.

[23] Orcina, "OrcaFlex 11.0d Documentation." Orcina Ltd, Daltongate, 2020.

[24] Orcina, "F01 Lowering hydrodynamics," *OrcaFlex User Group Meetings*. Orcina Ltd., Daltongate, 2013.

[25] API, *API RP 2SK: Design and Analysis of Stationkeeping Systems for Floating Structures*, 3rd ed. American Petroleum Institute, 2005.

[26] E. B. Djatmiko, *Perilaku dan Operabilitas Bangunan Laut di Atas Gelombang Acak*. Surabaya: ITS Press, 2012.

[27] "Navionics ChartViewer." Accessed: Dec. 11, 2023.

[Online]. Available: https://webapp.navionics.com/?lang=en#boating@7&key=pm%60a%40mokxU

[28] API, "API RP 2A: Recommended Practice for Planning, Designing and Constructing Fixed Offshore Platforms—Working Stress Design 21st edition," *American Petroleum Institute*. American Petroleum Institute, 2000.

[29] AISC, *Steel Construction Manual 13rd*, 13th ed. Chicago: American Institute of Steel Construction, 2005.

[30] S. F. Hoerner, *Fluid-Dynamic Drag*, 2nd ed. Washington D.C.: Hoerner, Sighard F., 1965.

[31] D. Å. Viki, "Limiting Operational Wave Criterion for Spool Installation Lift," Master's Thesis, University of Stavanger, Stavanger, 2015.

[32] S. D. Eri, "Analysis of Operability in Installing Heavy Subsea Modules," Master's Thesis, University of Stavanger, Stavenger, 2015.